

IMPACT OF MAJOR CORONAL MASS EJECTIONS ON GEOSPACE DURING 2005 SEPTEMBER 7–13

YUMING WANG,^{1,2} XIANGHUI XUE,¹ CHENGLONG SHEN,¹ PINZHONG YE,¹ S. WANG,¹ AND JIE ZHANG²

Received 2005 November 2; accepted 2006 March 24

ABSTRACT

We have analyzed five major CMEs originating from NOAA active region (AR) 808 during the period of 2005 September 7–13, when the AR 808 rotated from the east limb to near solar meridian. Several factors that affect the probability of the CMEs' encounter with the Earth are demonstrated. The solar and interplanetary observations suggest that the second and third CMEs, originating from E67° and E47°, respectively, encountered the Earth, while the first CME originating from E77° missed the Earth, and the last two CMEs, although originating from E39° and E10°, respectively, probably only grazed the Earth. On the basis of our ice cream cone mode and CME deflection model, we find that the CME span angle and deflection are important for the probability of encountering Earth. The large span angles allowed the middle two CMEs to hit the Earth, even though their source locations were not close to the solar central meridian. The significant deflection made the first CME totally miss the Earth even though it also had wide span angle. The deflection may also have made the last CME nearly miss the Earth even though it originated close to the disk center. We suggest that, in order to effectively predict whether a CME will encounter the Earth, the factors of the CME source location, the span angle, and the interplanetary deflection should all be taken into account.

Subject headings: solar-terrestrial relations — Sun: coronal mass ejections (CMEs)

1. INTRODUCTION

Predicting the potential geoeffectiveness of a coronal mass ejection (CME) has been an interesting and important topic in solar-terrestrial physics and space weather research. The characteristics of Earth-encountering CMEs, including the CME source location, width, speed, acceleration, interactions, etc., have been well studied. It was first suggested by Howard et al. (1982) that CMEs were directed toward or away from the Earth if they presented halo shapes in coronagraph images. Frontside halo CMEs, including partial halo CMEs (apparent width $\geq 120^\circ$), are Earth-directed (e.g., Hudson et al. 1998; Cane et al. 2000; St. Cyr et al. 2000). However, not all frontside halo CMEs will encounter the Earth. Only about half of all frontside halo CMEs have interplanetary counterparts detected near the Earth (e.g., Cane et al. 2000; Wang et al. 2002; Cid et al. 2004; Yermolaev et al. 2005).

The location of the surface source region of CMEs is probably the most important factor. Webb et al. (2000) showed that halo CMEs associated with surface activity within $0.5 R_\odot$ of Sun center appear to be an excellent indicator of increased geoactivity several days later. With more cases of halo CMEs, Cane et al. (2000) pointed out that the locations of the geoeffective CMEs should be within the longitude range of [E40°, W40°]. Further, Wang et al. (2002) and Zhang et al. (2003) found that there is an east-west asymmetry of the source region distribution of geoeffective CMEs with more geoeffective CMEs from the western hemisphere. Cane & Richardson (2003) found that about a third of the interplanetary CMEs detected in geospace were not preceded by a $>140^\circ$ halo CME.

There are other factors that can affect the probability of a CME encountering the Earth. The span angle is an evident one. A larger span angle should give a CME a higher probability of hitting the Earth. Another important factor is the CME deflection in the interplanetary medium (Wang et al. 2004). On the basis of

a statistical observational study and a theoretical model, Wang et al. (2004) concluded that the trajectory of a CME is affected by the background solar wind plasma and spiral magnetic field: fast CMEs will be deflected to the east and slow CMEs will be deflected to the west. If both the span angle and deflection factors are taken into account, the prediction of a CME's impact is more reliable. We demonstrate such a multifactor analysis in this paper.

A large solar active region, NOAA AR 808, rotated over the east limb on 2005 September 7 and subsequently produced a series of major flares detected in H α and soft X-rays. AR 808 was located at the southern hemisphere as seen in the magnetogram images obtained from the Michelson Doppler Imager (MDI; Fig. 1f) on board the *Solar and Heliospheric Observatory (SOHO)*. This region produced a total of nine X-class, 15 M-class, and many smaller X-ray flares³ from September 7 to 13 while it rotated from the eastern limb to central meridian. The X17.0 X-ray flare beginning at 17:17 UT on September 7 was the fifth largest X-ray flare ever observed. During this period, there were five major frontside CMEs along with several smaller CMEs, all originating from AR 808.

This series of successive major CMEs provides us an opportunity to study and compare their propagation in the interplanetary space and their impact on geospace, because they originated from the same source region. Such multiple fast frontside solar eruptions are expected to be very geoeffective. However, the quick-look Dst index from the World Data Center for Geomagnetism at Kyoto University showed that there was only one -123 nT storm, and for most of the time during the whole period the Dst index was larger than -100 nT. Why did these CMEs not cause great geomagnetic storms? Did some of these CMEs miss the Earth? These questions also draw our attention to these events. In the next section, the five major CMEs are presented, including the associated flares and their source locations. The identification of the interplanetary responses to these CMEs is

¹ School of Earth and Space Science, University of Science and Technology of China, Hefei, Anhui 230026, China; ymwang@ustc.edu.cn.

² School of Computational Sciences, George Mason University, 4400 University Drive, MSN 5C3, Fairfax, VA 22030.

³ See the report by the Space Environment Center, National Oceanic and Atmospheric Administration at <http://www.sel.noaa.gov/index.html>.

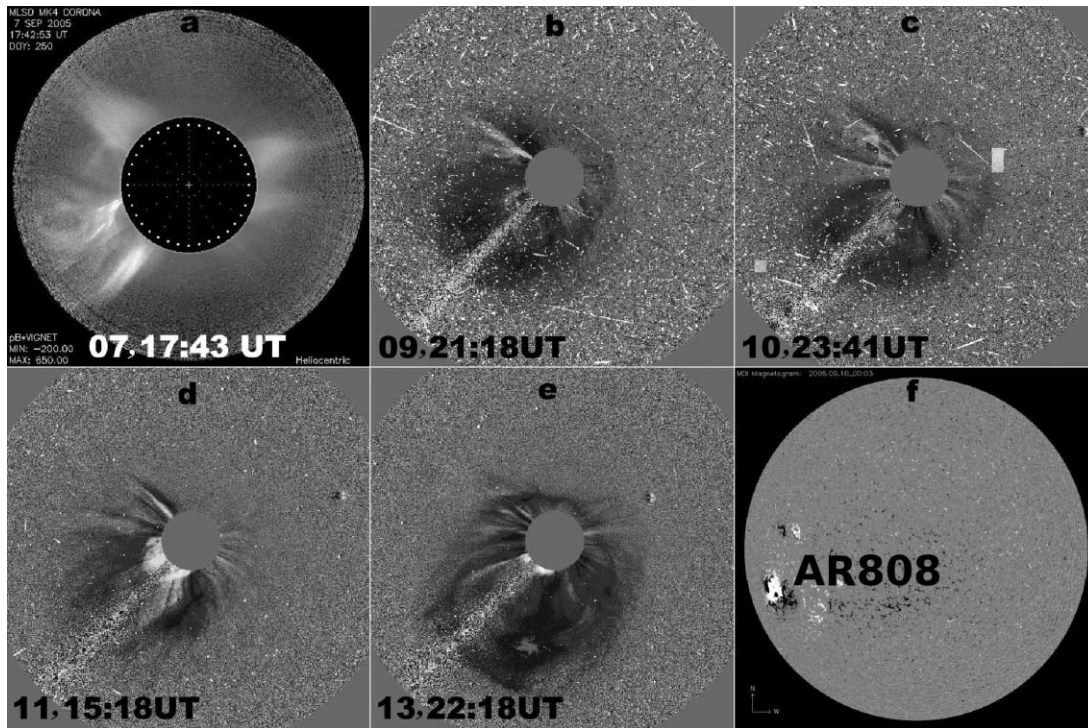


FIG. 1.—Five major CMEs observed during September 7–13 by (a) the MK4 coronameter of MLSO and (b–e) *SOHO* LASCO C3 coronagraph, and their source region AR 808 viewed in (f) *SOHO* MDI. The first event led to a large solar energetic particle (SEP) event that affected the LASCO detector through September 10, showing us a snow storm in the LASCO images (b) and (c).

made in § 3. In § 4, we investigate the CMEs' trajectories and their possible impact on geospace by using the CME models (ice cream cone model and deflection model). Discussion and conclusions are given in § 5.

2. MAJOR CORONAL MASS EJECTIONS DURING 2005 SEPTEMBER 7–13

2.1. Major CMEs

The Large Angle and Spectrometric Coronagraph (LASCO; Brueckner et al. 1995) on the *SOHO* spacecraft provides excellent observations of the corona above 2 solar radii. By examining the data from LASCO, four major halo CMEs can be clearly identified during the interested interval. Table 1 lists the time of their first appearance in the LASCO field of view. Figures 1b–1e show LASCO/C3 images of the CMEs. It should be noted that from ~11:00 on September 7 to ~12:00 UT on September 9, LASCO

was out of service and no data are available. Other observations are used to examine CMEs during the LASCO data gap.

First, the observations from MK4 coronameter⁴ at the Mauna Loa Solar Observatory (MLSO) are investigated. The field of view of the MK4 coronameter is from 1.1 to 2.8 R_{\odot} , different from that of LASCO/C2 from 2 to 6 R_{\odot} and LASCO/C3 from 3.7 to 32 R_{\odot} . Since MK4 coronameter is a ground-based instrument, it only covers a certain fraction of each day. Within the LASCO data gap, the MK4 obtained observations from about 17:00 to 20:00 UT on September 7, and from about 18:00 to 20:00 UT on September 8. The observations revealed that there was a bright CME at 17:35 UT on September 7 as shown in Figure 1a.

However, there are still two large data gaps from September 7 20:00 UT to September 8 18:00 UT and from September 8

⁴ See the description of this coronameter at <http://mlso.hao.ucar.edu/mk4.html>.

TABLE 1
LIST OF THE FIVE MAJOR CMEs FROM SEPTEMBER 7 TO 13

EVENT	CMEs				FLARES			TYPE II START TIME (UT)
	Day	Time ^a (UT)	Width ^b	V_p^c (km s^{-1})	Time ^d (UT)	Class	Location (deg)	
1.....	7	17:34	~160°	2534	17:17	X17.0	S11, E77	18:05
2.....	9	19:48	Halo	1942	19:13	X6.2	S12, E67	19:45
3.....	10	21:52	Halo	1102	21:30	X2.1	S13, E47	21:45
4.....	11	13:00	Halo	1360	12:44	M3.0	S16, E39	13:10
5.....	13	20:00	Halo	1366	19:19	X1.5	S9, E10	20:20

^a First appearance of CMEs in coronagraphs.

^b CME apparent width viewed in coronagraphs.

^c Projected speed of CMEs in the plane of the sky.

^d Onset time of associated X-ray flares.

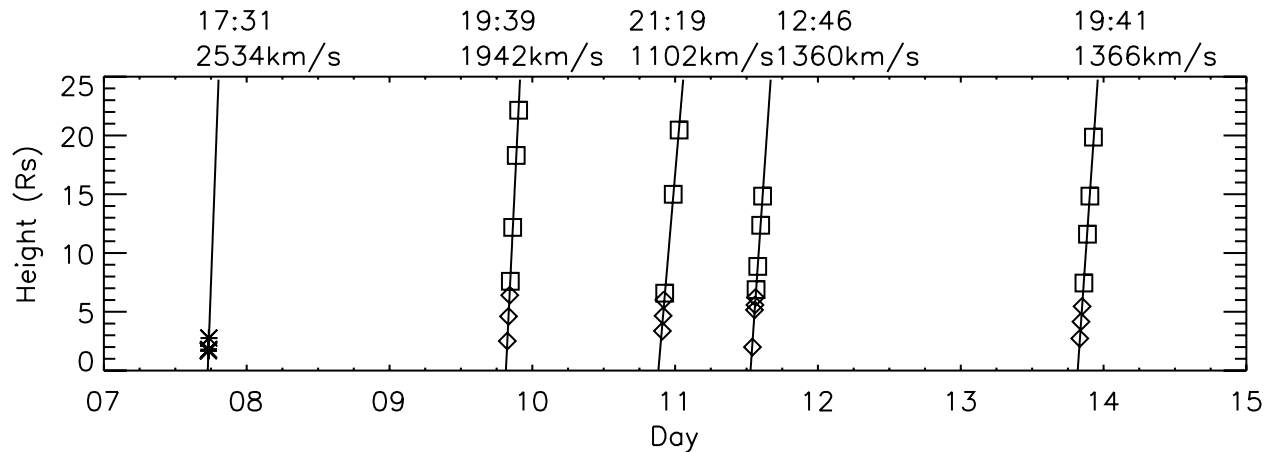


FIG. 2.—Height-time plots of the five major CMEs. The asterisks, diamonds, and squares denote the points measured in the MK4 coronameter and the C2 and C3 coronagraphs, respectively. The linear-fitted speeds are listed at the top, as well as the onset times inferred by extrapolating the height-time lines back to their associated flare locations.

20:00 UT to September 9 12:00 UT. In these two intervals, there were three X-class flares and six M-class flares, which implied the possibility of other major CMEs. The observations of solar radio bursts were used to detect CMEs during these periods. Type II radio bursts are thought to be an indicator of the presence of fast and wide CMEs. However, the wavelength band of the observations may be important. Gopalswamy et al. (2001, 2005) have shown that type II radio bursts appearing in the decameter-hectometric (DH) and kilometer bands are almost always associated with fast and wide interplanetary CMEs. Thus, DH to km band type II radio bursts can be used as a proxy of major frontside CMEs. The *Wind Waves* instrument provide such observations by RAD2 (1.075–13.825 MHz) and RAD1 (20–1040 kHz). The type II radio bursts observed by Waves can be found in the type II list⁵ compiled by Michael L. Kaiser. It indicates that there were only five type II radio bursts, whose start times were all consistent with the first appearances of the above five major CMEs detected in LASCO and the MK4 coronameter. M. L. Kaiser (2006, private communication) suggested that there was an event on September 8 beginning about 22:00 UT that might be a type II, but its signature is not clear, so it is not included in the list. This event was in the data gap. By checking the flare list, we find there was an X5.4 flare beginning at 20:52 UT on September 8 and ending at 21:17 UT that might be associated with the unclear burst. Even if there was a CME associated with this flare, we do not believe it was a major one, because of the uncertain type II radio burst.

In summary, the combination of the observations, including the images from LASCO and MK4 coronameter, the type II list from *Wind Waves* and the flare list from NOAA/SEC, suggests that there were in total five major CMEs during 2005 September 7–13. In the following subsection, we identify whether these CMEs were frontside, and where they originated from.

2.2. Identification of the Source Regions

The source region of a CME can be identified by examining the observations from the *SOHO* Extreme Ultraviolet Imaging Telescope (EIT; Delaboudiniere et al. 1995). Unfortunately, during the whole period of interest, there were no EIT data available. An alternative way to determine their source location is to associate these CMEs with reported flares.

The first major CME was observed only by the MK4 coronameter. It first appeared at 17:34 UT and traveled in the southeast

direction. The time and direction of this CME are both roughly consistent with those of the X17.0 flare originating from about S11° E77°. The height-time curve of this CME is plotted in Figure 2. By linearly extrapolating the height-time line back to the location of the associated flare, the CME onset inferred is at about 17:31 UT, near to the onset of the flare. Hence, this CME is most probably associated with this flare and can be considered a frontside event.

The other four major CMEs occurring on September 9, 10, 11, and 13 were all well observed by LASCO/C2 and C3. The C3 images (Figs. 1b–1e) indicate that they were all halo CMEs, and their major position angles were in the southeast direction. In the *GOES* (*Geostationary Operational Environmental Satellite*) X-ray time sequence, we find four large flares shortly before the first appearances of each of these CMEs. The onset times and locations of these flares are listed in Table 1. Using the same technique, we extrapolate the height-time profiles of these CMEs back to the flare locations (Fig. 2). It is found that the extrapolated CME onset time was within the time window of an hour centering on the flare beginning time. Thus, it is likely that these four flares were all associated with these four CMEs, which should all be considered frontside events.

As shown in Table 1, these CMEs are all fast and wide. Except for the first CME, which rose over the solar east limb, the other four CMEs all showed a halo shape that implies an Earth-directed propagation. Therefore these four CMEs should be expected to have ICME counterparts in geospace. Especially, the fourth and fifth CMEs should be able to impact the Earth because their location of AR 808 was less than 40° from the central meridian. Moreover, the occurrences of these major CMEs were all separated by more than 24 hr except one by ≈ 15 hours. Therefore, they were unlikely to merge into each other to form complex ejecta (Burlaga et al. 2001, 2002) or multiple magnetic-cloud structures (Wang et al. 2003, 2005) at 1 AU because of their short transit times and long separations.

3. INTERPLANETARY SHOCKS AND EJECTA ASSOCIATED WITH THESE CMEs

3.1. Corresponding Shocks of these CMEs

The interplanetary magnetic field and solar wind plasma measurements by the *Wind* spacecraft are used to analyze the interplanetary characteristics of these five major frontside CMEs. Figure 3 shows the interplanetary observations from September 7 to 17 covering the interval of the traversal of these CMEs from the Sun to the Earth. During this period, the *Wind* spacecraft was

⁵ Refer to <http://lep694.gsfc.nasa.gov/waves/typeII05.html>.

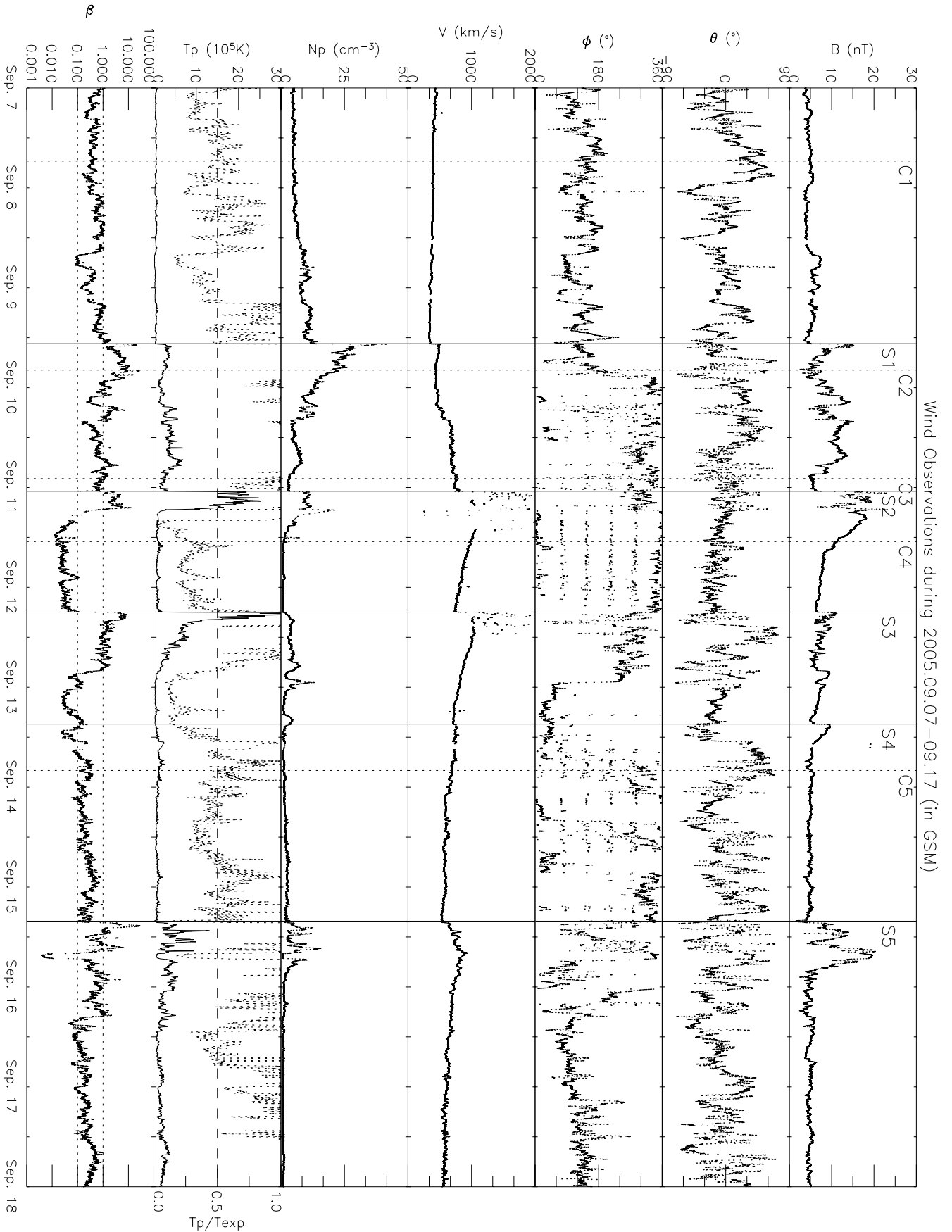


FIG. 3.—Interplanetary observations of *Wind* spacecraft during September 7–17.

at a distance of about $200 R_E$ away from the Earth toward the Sun. The first three panels show the magnetic fields including its magnitude and elevation and azimuthal angles in GSM (geocentric solar magnetic) coordinates. The other four panels present the solar wind speed, proton density and temperature, and β (the ratio of thermal pressure to magnetic pressure).

From this overview plot, one can find that there were five evident discontinuities appearing in the magnetic field strength, as marked by the five solid vertical lines. At the first, second, third, and fifth discontinuities, the solar wind speed, and proton density and temperature all increased suddenly and significantly, and hence these discontinuities were fast forward shocks. The fourth discontinuity looks like a pressure wave, might be not yet a shock, or might be a decayed fast shock, because only the speed and temperature increased slightly at that time (D. Berdichevsky 2006, private communication). In the following discussion, we use “shock” to refer to all of these five discontinuities for the sake of convenience.

Interplanetary shocks are usually driven by fast CMEs. Sometimes in situ observations exhibit an interplanetary shock without a fast interplanetary CME (ICME) behind it. This is because the driven shock can extend over a much wider angle than its driver, and the flank but not the nose of the shock passes through the observer, while the ICME itself might miss the observer (e.g., Cane 1988).

The high-speed solar wind streams from coronal holes can also drive shocks. However, usually only corotating interaction regions (CIRs) form between the fast and preceding slow streams within 1 AU. Shocks are rarely produced by such high-speed streams until beyond ~ 1 AU (Tsurutani et al. 1995). Thus, most interplanetary shocks detected near the Earth should be considered the products of fast CMEs.

On the basis of the above arguments, the associations between the five shocks and the CMEs should be well established, because there were only five major frontside CMEs from September 7 to 13. These CMEs, with projected speeds in the plane of the sky exceeding 1000 km s^{-1} , were all likely to drive a shock in the interplanetary medium. The numbers marked in Figure 3 indicate the CME-shock pairs. According to the first appearances of CMEs and the arrivals of shocks, the travel times (T) and average travel speeds (V) of shocks/ICMEs from the Sun to 1 AU are estimated. The travel times were 44, 29, 33, 44, and 37 hr, and the speeds V were therefore 948, 1425, 1277, 945, and 1141 km s^{-1} , respectively.

In addition, to make the established association between these CMEs and interplanetary shocks more convincing, we examined the LASCO images on September 14, because if there was a CME and it was fast enough, it might also have driven the fifth shock, which arrived at 08:12 UT on September 15. Fortunately, the LASCO images suggest that no major CME appeared on that day.

3.2. Presence/Absence of the ICMEs

Although the shocks driven by these fast CMEs were detected by the *Wind* spacecraft (i.e., these shocks impacted the Earth), it does not mean that the ICMEs, also called ejecta, the interplanetary counterparts of these CMEs, also impacted the Earth. For our purpose, we have used the following signatures to identify an ICME: the magnetic field magnitude is higher than that in the ambient environment, solar wind speed declines that indicates the expansion of ejecta, proton β is lower than ~ 0.1 (Farrugia et al. 1993; Tsurutani & Gonzalez 1995), proton temperature is less than half of the expected proton temperature T_{exp} (Richardson & Cane 1995). The expected temperature T_{exp} is calculated ac-

ording to an empirical formula obtained by Lopez & Freeman (1986):

$$T_{\text{exp}} = \begin{cases} (0.031V_{\text{sw}} - 5.1)^2, & V_{\text{sw}} < 500 \text{ km s}^{-1}, \\ 0.51V_{\text{sw}} - 142, & V_{\text{sw}} > 500 \text{ km s}^{-1}, \end{cases} \quad (1)$$

where T_{exp} is related to the solar wind speed V_{sw} . The ratio of proton temperature T_p to expected temperature T_{exp} is indicated by the dotted curve in the sixth panel of Figure 3. The criterion of $T_p/T_{\text{exp}} < 0.5$ was used in many studies (e.g., Richardson & Cane 1995; Wang & Richardson 2004; Berdichevsky et al. 2005).

Note that each individual signature is not the necessary condition. Some exceptions have been found (e.g., Gosling et al. 1987; Gosling 1990; Richardson et al. 1997). So, to be conservative, we identified an ejecta event only if all four criteria were satisfied. If only one or no signature is found, we consider there to be no ejecta. If two or three signatures are found, we consider this an ambiguous identification.

On the basis of Figure 3, there was no apparent ejecta detected following the first shock. After the first shock, the solar wind speed increased, and the values of T_p/T_{exp} and β were significantly larger than the expected values 0.5 and 0.1, respectively, although the magnetic field strength was strong. Three of the four signatures were not matched, so we believe that no ejecta could be identified after the first shock.

For the second and third events, all four signatures of ejecta are evident. The ejecta driving the second shock began at 06:54 UT on September 11, when the proton temperature and β decreased sharply and stayed at a very low level until the arrival of the next shock. During this period, the magnetic field strength was relatively strong, the solar wind speed decreased continuously, and the ratio of T_p/T_{exp} and proton β remained below 0.5 and 0.1, respectively.

The front boundary of the ejecta driving the third shock was at 20:57 UT September 12. The rear boundary is difficult to determine, but it could have been at 08:51 UT on the next day, i.e., the arrival of the next shock. Like with the previous ejecta, the magnetic field strength was relatively strong, the solar wind speed decreased continuously, and the ratio of T_p/T_{exp} and proton β were lower than approximately 0.5 and 0.1, respectively.

For the fourth shock, the signatures of its driver CME are weak. Two signatures are roughly satisfied. The profile of the solar wind speed behind the shock presents a weak expansion, and the temperature ratio fluctuated around the value of 0.5. The other two signatures were unsatisfied. The magnetic field strength was almost as strong as that of the ambient field, and the value of β was larger than 0.1 approximately. Thus, it is not clear that there was an ejecta following the shock. At best, only its flank was detected.

As to the last event, it is an interestingly complex one (I. Richardson & D. Berdichevsky 2006, private communication). The solar wind plasma and magnetic field suggest a sheath extending from the shock to about 7 UT on September 16. But the gradient in the profile of solar wind speed looks like a CIR. However, on September 15 from about 16:00 to 18:00 UT the proton temperature coincident with the low beta of the plasma could be interpreted as ejecta presence. A detailed study of this event is beyond the scope of this paper. Similar to the fourth event, no definite conclusion can be made. We tentatively believe that there was ICME material. If the structure between about 16:00 and 18:00 UT was an ejecta, the small passage time (~ 2 hours) implies that only its flank was observed by the *Wind* spacecraft; i.e., this ICME probably only grazed the Earth.

TABLE 2
ASSOCIATED INTERPLANETARY SHOCKS AND POSSIBLE ICME EJECTA

Shock	Time ^a	ICME	T^b	V^c
1.....	9 13:27	No	44	948
2.....	11 00:54	Yes	29	1425
3.....	12 05:57	Yes	33	1277
4.....	13 08:51	Flank?	44	945
5.....	15 08:12	Flank?	37	1141

^a Time of shock arrival at 1 AU, along with date (in 2005 September).

^b Interval between the extrapolated onset of a CME to the arrival of the associated shock. This is used as the travel time of a CME from Sun to the Earth.

^c Average travel speed of a CME derived from 1 AU/ T .

The interplanetary responses to these five major CMEs are summarized in Table 2. One major CME missed the Earth at 1 AU, two probably grazed the Earth, and two encountered the Earth. It is interesting to note that the fifth CME, which originated from near the center ($\sim E10^\circ$) of the solar disk, did not impact the Earth head-on as might have been expected. The following section gives a possible explanation of the above results.

4. MODELED CME PROPERTIES AND THEIR EFFECT ON IMPACT

4.1. Ice Cream Cone Model

Most CMEs look like cone-shaped blobs in a coronagraph. Studies on broadside CMEs, in which the projection effect should be almost eliminated, suggest that the observed span angles of these CMEs remain nearly constant (Webb et al. 1997; Schwenn et al. 2005), and their motion is almost radial through the LASCO C2 and C3 fields of view. Thus, many researchers suggest that the geometrical properties of most CMEs could be inferred indirectly by a cone model (Howard et al. 1982; Fisher & Munro 1984; Leblanc et al. 2001; Zhao et al. 2002; Michalek et al. 2003; Xie et al. 2004). Recently, an ice cream cone model was further developed by Xue et al. (2005), whose work showed consistency between the fitted and observed speeds of CMEs.

Assuming that the ice cream cone model is suitable for the September CMEs, we deduce the real span angles of them. Figure 4 shows an example (using the last event) of our process. First, on the LASCO image, we plot several radial lines from the solar center as measurement directions, and we mark the CME leading edge along each direction. Since there is a sufficient number of LASCO images for this CME, its projected speeds at all the given directions can be obtained by fitting the measured height-time curves with linear lines. Second, assuming that this CME originated from the associated flare location, we can use the equations listed in Table 1 of the Xue et al. (2005) paper to fit the measured projected speeds with the ice cream cone model, in which the span angle is fitted as a parameter. The least-squares fit is applied to get the best solution, as shown in Figure 5.

In Figure 5, ψ along the x -axis denotes the position angle measured counterclockwise from solar north in degrees in LASCO images. The triangles indicate the measured projected speeds of CMEs along each position angle. The curves show the fitted results. As indicated in the plots, the goodness-of-fit is evaluated by the rms deviation $[\sum (V_f - V_m)^2/N]^{1/2}$, where V_f and V_m are the fitted and measured projected CME speeds, respectively, normalized by the modeled CME speed. One can find that the outlines of the measured points of the last two CMEs are roughly matched. The fitting is especially good for the last one, in which the rms deviation is only 0.08. However, for the other two CMEs,

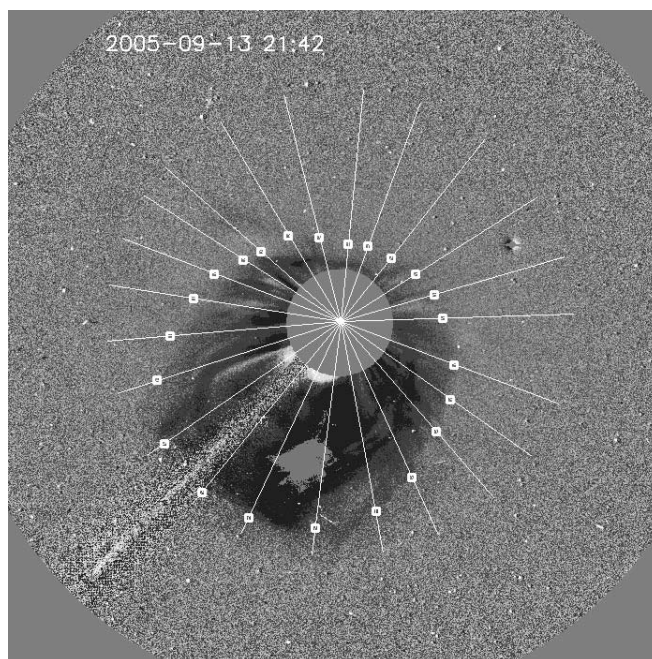


FIG. 4.—Running-difference image of the CME on September 13. The radial lines show the directions of the measurements, and the squares show the leading edge of the CME along these directions.

the deviations between the model and observations are somewhat larger. We believe this is probably because the shapes of these two CMEs were not particularly well described by a cone.

For the first CME, which was a limb event, the span angle is measured directly from the MK4 coronameter observations. The deduced span angles of these five CMEs have been listed in the second column of Table 3. One can find that four of the five CMEs had very large span angles. The wide span angle should increase the probability that a frontside CME would impact the Earth.

4.2. Deflected Propagation of CMEs in the Interplanetary Medium

As long as the source location and the span angle of a CME are known, whether it can impact the Earth can be estimated. The deflection of propagation in the heliosphere should be also taken into account. Wang et al. (2002) found that the distribution of the solar source regions of Earth-directed CMEs has east-west asymmetry, which was further confirmed by Cane & Richardson (2003), Zhang et al. (2003), and Wang et al. (2004). Particularly, in the Wang et al. (2004) paper, this east-west asymmetry is well explained by the deflection of CMEs' propagation in the heliosphere. Under the constraint of the interplanetary spiral magnetic field and the background solar wind, a CME faster than background solar wind would be deflected to the east, whereas a CME slower than background solar wind would be deflected to the west. A kinetic model (Wang et al. 2004) was proposed to describe such behavior as given by the formula

$$\Delta\Phi = \left(\frac{1}{a} - \frac{1}{a_0}\right)r, \quad (2)$$

where r is given by

$$\frac{1}{2a} \left[r\sqrt{r^2 + a^2} + a^2 \ln\left(r + \sqrt{r^2 + a^2}\right) \right] - \frac{a}{2} \ln a = 1 \text{ AU}. \quad (3)$$

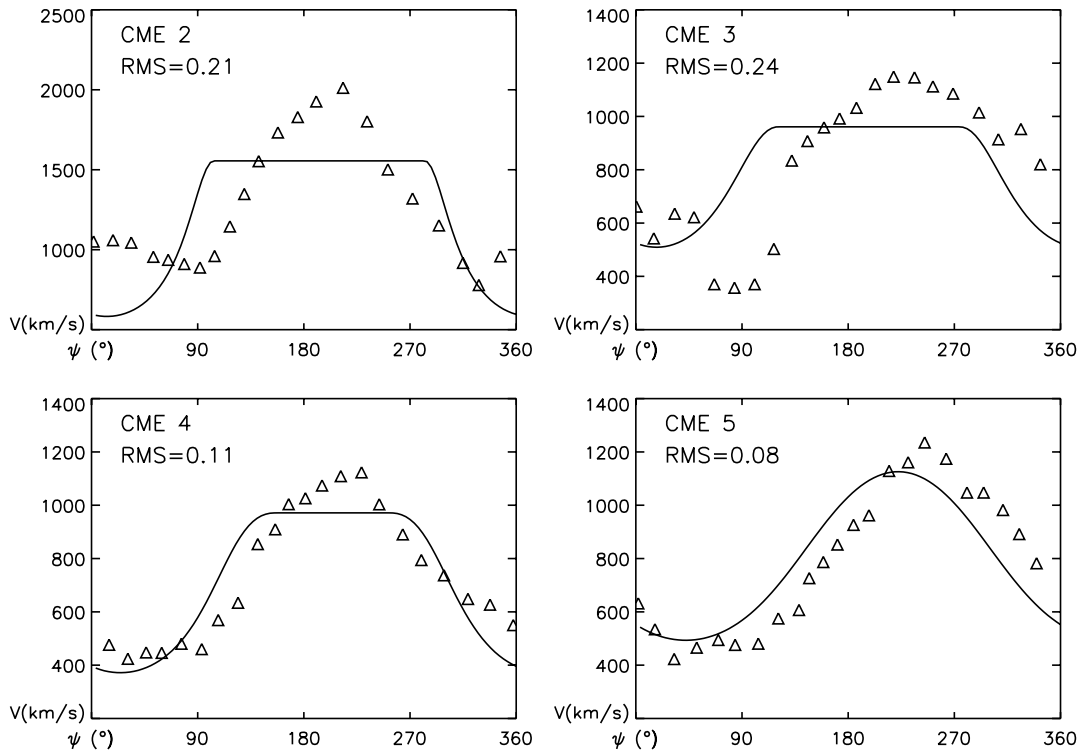


FIG. 5.—Fits of CME projected speeds using the ice cream cone model. See text for explanation.

Here $a = V/\Omega$, $a_0 = V_{sw}/\Omega$, V is the CME speed, V_{sw} is the background solar wind speed, $\Omega = 2.7 \times 10^{-6} \text{ rad s}^{-1}$ is the angular speed of the solar rotation, and $\Delta\Phi$ is the calculated deflection angle at 1 AU. If $\Delta\Phi > 0$, a CME deflects toward the west. From the formula, the deflection angle depends on the CME speed and background solar wind speed.

To use the formula, one needs to know the CME speed in interplanetary space. One can get the projected speed of CMEs by measuring the CMEs' leading edge in LASCO fields of view, but this speed may depart largely from the real CME speed in the heliosphere. One also can obtain the modeled speed of CMEs by applying the cone models. Perhaps this speed is closer to the real CME speed, but it is only valid within several tens solar radii. Slow CMEs are accelerated and fast CMEs are slowed down in interplanetary medium (e.g., Gopalswamy et al. 2000; Rust et al. 2005). Due to the complicated interactions between CMEs and the solar wind, the interplanetary acceleration of CMEs has not

been fully addressed. Considering that a CME's propagation from the Sun to 1 AU is a large-scale and long-duration phenomenon, the average travel speed of CMEs is adopted as a first-order approximation. The average travel speed is calculated in terms of the intervals between the extrapolated onset of CMEs to the arrival of the associated shocks (see the last column of Table 2).

The background solar wind speed V_{sw} ahead of each CME is taken from the *Wind* measurements as shown in Figure 3. The solar wind speeds ahead of the shocks are considered to be the background speeds for the CMEs. Thus, the values of V_{sw} for these five CMEs are about 400, 700, 700, 700, and 500 km s^{-1} , respectively. Using equation (2), the deflection angles of these CMEs at 1 AU are therefore calculated and listed in Table 3. The largest deflection is for the first CME, with $\Delta\Phi = -33^\circ$. This is because (1) it was embedded in the slowest background solar wind, which provided the strongest resistance and made the CME shift aside, and (2) the travel speed, implying the kinetic energy of this CME, was less than those of the second, third, and fifth CMEs, so that its propagation path can be changed more easily. The first factor is more important than the second one. This is evident because the fourth CME, whose travel speed was comparable to that of the first CME, was almost not deflected ($\Delta\Phi = -8^\circ$). The deflection angles of the second, third, and fifth CMEs were -17° , -15° , and -26° , respectively.

Figure 6 shows the motion of these CMEs and their spans in longitude on the ecliptic plane for the case of deflected propagation and for the case of radial propagation. The colored dashed radial and solid spiral lines represent the trajectories of the central axis of each CME in terms of whether it moves out radially or is deflected, respectively. The colored arcs at 1 AU denote the longitude ranges over which these CMEs could sweep. It is found that if there were no deflection, almost all of the CMEs would impact the Earth because of their large span angles, even

TABLE 3
MODELED CME SPAN ANGLES AND CME DEFLECTIONS
IN THE HELIOSPHERE

Event	Span Angle ^a (deg)	V_{sw} ^b	$\Delta\Phi$ (deg)
1.....	~160	400	-33
2.....	179	700	-17
3.....	161	700	-15
4.....	128	700	-8
5.....	63	500	-26

^a The modeled span angle of a CME by the ice cream cone model.

^b The background solar wind speed ahead of each CME.

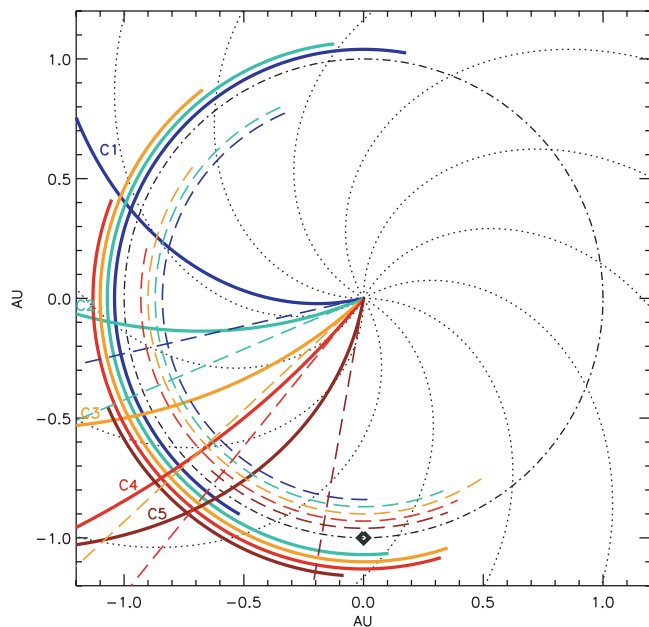


FIG. 6.—Motion of the CMEs and their spans in longitude on the ecliptic plane. The dashed (solid) lines indicate the CME motion without (with) deflections. The dot-dashed circle marks the distance of 1 AU. The dotted spiral lines indicate the undisturbed interplanetary magnetic field lines when the solar wind speed is equal to 450 km s^{-1} . The location of the Earth is marked by the diamond.

the first CME that originated from near the east limb. Moreover, the last CME should encounter the Earth head-on because its source region location is $\sim E10^\circ$, near the solar central meridian.

However, when the deflection effect is taken into account, the trajectories of these CMEs are changed significantly. The first CME completely missed the Earth. The last CME almost missed the Earth. Compared to radial propagation, the deflection effect on these two CMEs is very significant in terms of their hitting or missing the Earth. Certainly, for the last CME, its relatively narrow span is also a factor. As to the three CMEs in between, they could still encounter the Earth in the deflection situation thanks to their large span angles, but the ejecta only grazed the Earth.

5. CONCLUSIONS AND DISCUSSION

In summary, we studied five major CMEs occurring from 2005 September 7 to 13 and their counterparts near the Earth. The solar observations show that these five CMEs from the frontside of the Sun were all fast and wide. The interplanetary observations from the *Wind* spacecraft show that there were just five corresponding shock structures at 1 AU during this period. Among these five events, the second and third shocks were observed to be followed by the interplanetary counterpart of the CMEs. However, the first shock was not followed by an ejecta. In the last two CMEs the presence of an ejecta was ambiguous. We suggest that, even if the ICME ejecta for the two ambiguous events passed through the Earth orbit, they only passed by with their flanks at best. This is particularly interesting for the last CME, whose source region is directly toward the Earth, but there was no clear ICME signature near the Earth.

By combining the ice cream cone model (Xue et al. 2005) and CME deflection model (Wang et al. 2004), we find that besides the obvious factor of the source region location, the span angle and the deflection are also important in determining the probability of a CME impacting an object such as the Earth. The large

span angles of some CMEs (e.g., the second, third, and possible fourth) account for the fact that they are observed by the *Wind* spacecraft (i.e., they hit the Earth), even though their source region locations are not close to the solar central meridian. The significant deflection makes the first CME completely miss the Earth although it also had wide span angle. The deflection makes the last CME almost miss the Earth, even though it originated near solar central meridian.

Although the model is supported by the observations in these five cases, the uncertainty in estimating CME parameters should be noted. One may note that the calculated deflection angles of the first four CMEs are relatively small compared with their span angles. According to the rms deviations marked in Figure 5, the fits for the second and third CMEs are relatively poor. The estimated span angles for them might not be so accurate. However, these CMEs must be larger than 134° for the second CME and 94° for the third CME to ensure the CMEs' encounter with the Earth on the basis of their source region locations. When the deflection effect is considered, the span angle should be even larger.

The deflection effect is most evident for the last CME. The fit to the cone model for this CME is the best (rms = 0.08), and the deflection of it is also the most significant. The ratio of the deflection angle to its span angle is about $26/63 \sim 41\%$. Even though this CME was expected to encounter the Earth directly because it originated from near the center of solar surface, our model explains the unexpected fact that this CME did not pass the Earth head-on.

In this paper, we discuss the major CMEs only. According to the CME list⁶ compiled by Guillermo Stenborg at Naval Research Laboratory (NRL), there were many minor CMEs due to the extreme activity of AR 808. These CMEs were all nonhalo ones, and most of them were even faint. One can imagine that the span angles and speeds of these CMEs should be less than those of the five major CMEs. Thus, these minor CMEs are unlikely to be the drivers of the shocks during September 9–15.

In addition, we can find that some previous observational results do directly or indirectly support our conclusion obtained here. The 1997 April 22 flux rope, for example, reported by Webb et al. (2000) was probably the counterpart of a backside partial halo CME on April 16, which was also mentioned in Zhang et al. (2003). In addition to this event, Zhang et al. (2003) also reported other three similar events, in which the ICME ejecta clearly detected in the geospace were associated with extremely slow CMEs coming out from the eastern limb without obvious source region on the front disk. This “mysterious” phenomenon can be explained by our model, which predicts that a very slow CMEs from eastern limb may encounter the Earth. Moreover, Schwenn et al. (2005) showed that in 15% of comparable cases, a full or partial halo CME does not cause any ICME signature at Earth at all, and on the other hand 20% of transient shocks or ICMEs or isolated geomagnetic storms are not caused by an identifiable partial or full halo CME from the frontside. Their study suggests that a nonfrontside halo CME might encounter the Earth, and a frontside halo CME might miss the Earth. To answer the question whether a CME will encounter the Earth or not, all factors should be considered, including the source region location, the span angle, and the deflection in the interplanetary medium.

This paper suggests that the deflection effect may be an important factor in space weather predictions. In the present stage, the analytical CME deflection model is highly simplified, in which

⁶ See the link ftp://lasco6.nascom.nasa.gov/pub/lasco/status/LASCO_CME_List_2005.

the force of interplanetary magnetic field is dominant and only the speeds of the CME and solar wind are taken into account. Other factors, such as the momentum exchange, the distortion of the magnetic field configuration in both CME body and interplanetary medium, and so on, are totally ignored. Thus, the estimated deflected trajectories of CMEs may not be accurate. To fully assess the kinematics and possible deflections of CMEs in the interplanetary medium, a more sophisticated model, such as a full MHD code, is needed.

We acknowledge the use of the solar data from the LASCO and MDI instruments on board *SOHO* spacecraft and from the MK4 coronameter at Mauna Loa Solar Observatory, and the interplanetary data from *Wind* spacecraft. The *SOHO* LASCO

data used here are produced by a consortium of the Naval Research Laboratory (USA), Max-Planck-Institut für Aeronomie (Germany), Laboratoire d'Astronomie (France), and the University of Birmingham (UK). *SOHO* is a project of international cooperation between ESA and NASA. We also acknowledge the use of solar event reports compiled by the Space Environment Center of NOAA. We thank Michael L. Kaiser for the comment on type II radio bursts, and thank Ian Richardson and Daniel Berdichevsky for comments on the interplanetary solar wind observations. We thank Ken Dere for improving the language. The authors except J. Zhang are supported by the National Natural Science Foundation of China (40525014, 40404014, 40336052, 40336053), the Chinese Academy of Sciences (KZCX3-SW-144 and startup fund), and the Program for New Century Excellent Talents in University (NCET-04-0578).

REFERENCES

- Berdichevsky, D. B., Richardson, I. G., Lepping, R. P., & Martin, S. F. 2005, *J. Geophys. Res.*, 110, A09105
- Brueckner, G. E., et al. 1995, *Sol. Phys.*, 162, 357
- Burlaga, L. F., Plunkett, S. P., & St. Cyr, O. C. 2002, *J. Geophys. Res.*, 107, 1266
- Burlaga, L. F., Skoug, R. M., Smith, C. W., Webb, D. F., Zurbuchen, T. H., & Reinard, A. 2001, *J. Geophys. Res.*, 106, 20957
- Cane, H. V. 1988, *J. Geophys. Res.*, 93 (A1), 1
- Cane, H. V., & Richardson, I. G. 2003, *J. Geophys. Res.*, 108 (A4), 1156
- Cane, H. V., Richardson, I. G., & St. Cyr, O. C. 2000, *Geophys. Res. Lett.*, 27, 3591
- Cid, C., Hidalgo, M. A., Saiz, E., Cerrato, Y., & Sequeiros, J. 2004, *Sol. Phys.*, 223, 231
- Delaboudiniere, J.-P., et al. 1995, *Sol. Phys.*, 162, 291
- Farrugia, C. J., Burlaga, L. F., Osherovich, V. A., Richardson, I. G., Freeman, M. P., Lepping, R. P., & Lazarus, A. J. 1993, *J. Geophys. Res.*, 98 (A5), 7621
- Fisher, R. R., & Munro, R. H. 1984, *ApJ*, 280, 428
- Gopalswamy, N., Aguilar-Rodriguez, E., Yashiro, S., Nunes, S., Kaiser, M. L., & Howard, R. A. 2005, *J. Geophys. Res.*, 110, A12S07
- Gopalswamy, N., Lara, A., Lepping, R. P., Kaiser, M. L., Berdichevsky, D., & St. Cyr, O. C. 2000, *Geophys. Res. Lett.*, 27, 145
- Gopalswamy, N., Yashiro, S., Kaiser, M. L., Howard, R. A., & Bougeret, J. L. 2001, *J. Geophys. Res.*, 106 (A12), 29219
- Gosling, J. T. 1990, in *Physics of Magnetic Flux Ropes*, ed. C. T. Russell, E. R. Priest, & L. C. Lee (Geophys. Monogr. 58; Washington: AGU), 343
- Gosling, J. T., Baker, D. N., Bame, S. J., Feldman, W. C., Zwickl, R. D., & Smith, E. J. 1987, *J. Geophys. Res.*, 92, 8519
- Howard, R. A., Michels, D. J., Sheeley, N. R., Jr., & Koomen, M. J. 1982, *ApJ*, 263, L101
- Hudson, H. S., Lemen, J. R., St. Cyr, O. C., Sterling, A. C., & Webb, D. F. 1998, *Geophys. Res. Lett.*, 25, 2481
- Leblanc, Y., Dulk, G. A., Vourlidas, A., & Bougeret, J.-L. 2001, *J. Geophys. Res.*, 106, 25301
- Lopez, R. E., & Freeman, J. W. 1986, *J. Geophys. Res.*, 91, 1701
- Michalek, G., Gopalswamy, N., & Yashiro, S. 2003, *ApJ*, 584, 472
- Richardson, I. G., & Cane, H. V. 1995, *J. Geophys. Res.*, 100 (A12), 23397
- Richardson, I. G., Farrugia, C. J., & Cane, H. V. 1997, *J. Geophys. Res.*, 102, 4691
- Rust, K., Anderson, B. J., Andrews, M. D., Acuna, M. H., Russell, C. T., Schuck, P. W., & Mulligan, T. 2005, *ApJ*, 621, 524
- Schwenn, R., Dal Lago, A., Huttunen, E., & Gonzalez, W. D. 2005, *Ann. Geophys.*, 23, 1033
- St. Cyr, O. C., et al. 2000, *J. Geophys. Res.*, 105, 18169
- Tsurutani, B. T., & Gonzalez, W. D. 1995, *J. Atmos. Terr. Phys.*, 57, 1369
- Tsurutani, B. T., Gonzalez, W. D., Gonzalez, A. L. C., Tang, F., Arballo, J. K., & Okada, M. 1995, *J. Geophys. Res.*, 100 (A11), 21717
- Wang, C., & Richardson, J. D. 2004, *J. Geophys. Res.* 109, A06104
- Wang, Y. M., Ye, P. Z., & Wang, S. 2003, *J. Geophys. Res.*, 108 (A10), 1370
- Wang, Y. M., Ye, P. Z., Wang, S., Zhou, G. P., & Wang, J. X. 2002, *J. Geophys. Res.*, 107 (A11), 1340
- Wang, Y., Shen, C., Ye, P., & Wang, S. 2004, *Sol. Phys.*, 222, 329
- Wang, Y., Zheng, H., Wang, S., & Ye, P. 2005, *A&A*, 434, 309
- Webb, D. F., Cliver, E. W., Crooker, N. U., St. Cyr, O. C., & Thompson, B. J. 2000, *J. Geophys. Res.*, 105 (A4), 7491
- Webb, D. F., Kahler, S. W., McIntosh, P. S., & Klimchuck, J. A. 1997, *J. Geophys. Res.*, 102 (A11), 24161
- Xie, H., Ofman, L., & Lawrence, G. 2004, *J. Geophys. Res.*, 109, A03109
- Xue, X. H., Wang, C. B., & Dou, X. K. 2005, *J. Geophys. Res.*, 110, A08103
- Yermolaev, Y. I., Yermolaev, M., Zastenker, G., Zelenyi, L., Petrukovich, A., & Sauvaud, J.-A. 2005, *Planet. Space Sci.*, 53, 189
- Zhang, J., Dere, K. P., Howard, R. A., & Bothmer, V. 2003, *ApJ*, 582, 520
- Zhao, X. P., Plunkett, S. P., & Liu, W. 2002, *J. Geophys. Res.*, 107 (A8), 1223